High Power Laser Science and Engineering, (2026), Vol. 14, e70, 13 pages.
doi:10.1017/hpl.2026.10160

HIGH POWER LASER SCIENCE AND ENGINEERING

RESEARCH ARTICLE

High-stability and high-efficiency pulse compression technology based on high-repetition-rate transient self-pumped Brillouin scattering‡

Chen Cao[1,2], Yulei Wang[1,2], Qifan Dang[1,2], Linru He[1,2], Jianfeng Yue[1,2], Hengzhe Yu[1,2], Yu Yu[1,2], Zhenxu Bai[1,2], and Zhiwei Lv[1,2]

[1] *Center for Advanced Laser Technology, Hebei University of Technology, Tianjin, China*

[2] *Hebei Key Laboratory of Advanced Laser Technology and Equipment, Tianjin, China*

(Received 14 March 2026 UTC; revised 22 April 2026 UTC; accepted 20 May 2026 UTC)

Abstract

High-repetition-rate and high-stability short-pulse lasers have broad application prospects in large-scale integrated equipment serving industrial manufacturing and scientific research. Pulse compression techniques based on transient stimulated Brillouin scattering (SBS) are an effective means of obtaining short-pulse lasers. The transient effects and thermal breakdown enhancement effects in the high-repetition-rate transient SBS process will cause significant gain attenuation, resulting in a decrease in output energy reflectivity and stability. In this study, we proposed a pulse compression technique based on transient self-pumped Brillouin scattering (SPBS). By combining pump intensity attenuation with gain compensation based on a self-feedback seed model, the transmission loss and sound field intensity fluctuations during scattering were significantly reduced. The experiment verified the compression capability of the transient SPBS, which improved the output energy reflectivity and stability. The results showed that at a repetition rate of 300 Hz, the transient SPBS had a maximum energy reflectivity of 96.5% and an output energy of 24.1 mJ. Without the interference of the breakdown effect, a stable pulsed laser output with an energy relative standard deviation of only 1.42%, a time-domain duration of 225 ps and a peak power of over 100 MW was finally obtained. Our research provides a valuable reference for the generation of high-repetition-rate, high-peak-power lasers.

Keywords: high efficiency; high repetition rate; high stability; pulse compression; self-pumped Brillouin scattering

1. Introduction

High-repetition-rate and high-stability short-pulse lasers are widely used in industrial processing, inertial fusion energy (IFE), optoelectronic material modification and microscopic imaging[1–5]. Transient stimulated Brillouin scattering (SBS) pulse compression technology has been proven to obtain short-pulse lasers of less than 100 ps[6,7]. Due to its advantages such as low generation threshold and high scattering intensity[8,9], it can easily achieve extremely high compression ratios[10–12]. Currently, experimental results approaching the theoretical compression limit have been reported[13,14]. However, as the repetition rate and pump intensity of lasers continue to increase, the thermal and intensity load capacity of transient SBS are challenged. Under the combination of transient effects and thermal breakdown enhancement effects, the energy reflectivity and stability of Stokes light are severely degraded[15–19]. Researchers have proposed some practical methods to try to alleviate heat accumulation in the focal region, such as ultrafiltration technology targeting impurity molecules[20], rotating off-centered lens technology[21] and high-viscosity media[22–24]. However, these methods have only achieved valuable improvements in high-repetition-rate steady-state SBS, and the results of their application in transient SBS are still unknown. The key reason for the degradation of the output characteristics of high-repetition-rate transient SBS is that the high-repetition-rate pump light always excites the acoustic field for energy transfer in a focused state. The extremely high pump intensity and temperature at the focal point directly destroy the chemical bonds between Brillouin medium molecules, generating

Correspondence to: Y. Wang, Center for Advanced Laser Technology, Hebei University of Technology, Tianjin 300401, China. Email: wyl@hebut.edu.cn

‡ This article has been updated since its original publication. A notice detailing this can be found here: https://doi.org/10.1017/hpl.2026.10196.

© The Author(s), 2026. Published by Cambridge University Press in association with Chinese Laser Press. This is an Open Access article, distributed under the terms of the Creative Commons Attribution licence (https://creativecommons.org/licenses/by/4.0), which permits unrestricted re-use, distribution and reproduction, provided the original article is properly cited.

https://doi.org/10.1017/hpl.2026.10160 Published online by Cambridge University Press

a photoionization effect that produces a large amount of plasma and a large number of electrons. These substances will absorb a large number of pump photons, causing the internal temperature of the medium to continue to rise. This cycle will continue until thermal equilibrium is reached. Meanwhile, the transient effect causes a sharp increase in the number of transmitted pump photons during the acoustic field establishment process. The combined effect of these two factors, leading to increased system losses and decreased stability, has a devastating impact on the scattering process.

In 2003, Guo *et al.*[25] first proposed the 'self-feedback seed model' of SBS, namely self-pumped Brillouin scattering (SPBS). This method does not require a focusing structure: the pump light transmitted in parallel will be collinearly reflected in a certain proportion after passing through the medium cell. Stokes photons in the Brillouin linewidth range of the pump light spectrum will interact with pump photons and excited phonons, which is equivalent to injecting a fixed intensity of Stokes seed light in the reverse direction. In 2011, Dement'ev *et al.*[26] achieved an experiment on SPBS pulse compression based on the interaction between feedback light and forward pump light, and the results showed that its energy stability was significantly better than that of traditional SBS. Zhu *et al.*[27] and Wang *et al.*[28] successively achieved output energy exceeding the joule level under high-reflectivity conditions based on SPBS. Among these, Zhu *et al.*[27] used pump light with a pulse width of 3 ns and, under the condition of an injected pump energy of 4.16 J (peak power of 1.39 GW), obtained the shortest compressed laser output of about 310 ps, with a compression ratio of about 9.7 times. Wang *et al.*[28] used a pump light with a pulse width of 5 ns and an injected pump energy of 5.36 J (peak power of 1.07 GW) to obtain a compressed laser output of about 360 ps, with a compression ratio of about 13.9 times. The above results demonstrate the unique advantages of SPBS technology in improving output energy and stability. However, all the results reported so far have been verified in low-repetition-rate (1–10 Hz) steady-state SBS (pump pulse width approximately tens of nanoseconds), and require the pump light energy to reach the level of hundreds of millijoules, which is technically difficult.

In this study, we establish a theoretical model of transient SPBS based on pump intensity decay. The evolution of the normalized proportion η of the initial Stokes component in the pump light spectrum is simulated. We design a high-repetition-rate transient SPBS pulse compression system and experimentally investigate the relationship between the SPBS output characteristics and the pump pulse parameters and other key influencing factors. The results demonstrate that transient SPBS achieved a compression ratio exceeding two times that of SBS with an injection energy of only 30 mJ, and its peak pump power was more than 20 times lower than that reported in previous work. By comparing the results with those of SBS under the same conditions, the absolute advantage of transient SPBS in terms of energy reflectivity and stability is clearly demonstrated. Ultimately, a short-pulse laser with a peak power exceeding 100 MW@300 Hz is obtained with less than 5% system loss and an energy relative standard deviation (RSD) of 1.42%. We hope that this research will provide valuable assistance for the application of transient SPBS in high-repetition-rate, high-reliability laser systems.

2. Theory

Brillouin scattering is essentially a third-order nonlinear effect with threshold characteristics. The pump field, Stokes field and phonon field must satisfy the laws of conservation of momentum and energy. When a Brillouin elastic medium is irradiated by pump light, it will generate an initial phonon field and seed light. When the amplitude of the sound field is weak, the scattering intensity and efficiency are very low, and it is in the spontaneous Brillouin scattering stage. As the pump intensity increases, when the ratio of seed light intensity to pump light intensity is greater than 10^{-12}, the stimulated scattering stage begins[29]. Scattering efficiency and intensity increase exponentially with increasing pump intensity. The most efficient energy transfer can only be achieved when the difference between the frequency of pump light and the frequency of Stokes light equals the phonon frequency (Brillouin shift). To achieve higher scattering efficiency, the traditional SBS process employs focusing structures to increase pump intensity, thereby enhancing the initial intensity of the Stokes seed light. However, under a high repetition rate and strong pumping, thermally induced breakdown enhancement effects are likely to occur in the focal region.

SBS originates from acoustic phonon vibrations, the phonon frequency is relatively low and the Brillouin frequency shift of the common liquid Brillouin medium is only 1–2 GHz. When the pump pulse width is short enough, theoretically the normalized intensity ratio of the Stokes component within the Brillouin linewidth in the spectrum to the main frequency can reach the threshold intensity ratio (10^{-12}) of stimulated scattering. Therefore, even in a non-focused structure, the pump light can still compensate for the gain attenuation caused by the reduction in pump intensity by relying on the interaction with the Stokes light component in its own spectrum, thus achieving the pulse width compression process. We propose a pulse compression technique based on transient SPBS, the physical mechanism and process of which are shown in Figure 1. The spectrum of a short-pulse pump light with a main frequency of ω_p contains a certain proportion of Stokes components with a frequency of ω_s. The pump light enters the Brillouin medium cell in parallel, exciting the electrostriction effect to

https://doi.org/10.1017/hpl.2026.10160 Published online by Cambridge University Press

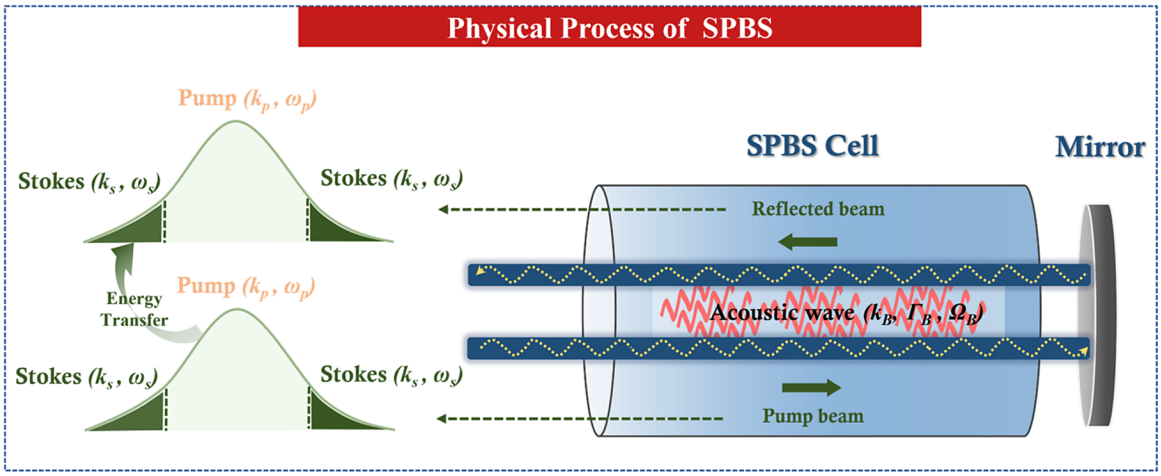


Figure 1. Schematic diagram of the SPBS principle.

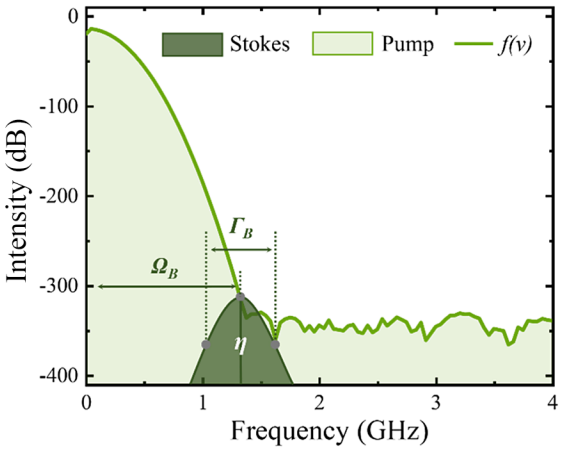


Figure 2. Schematic diagram of the pump spectrum and η.

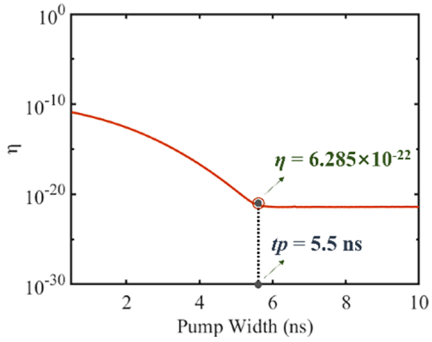


Figure 3. Variation of η with pump pulse width.

generate an acoustic phonon field with a main frequency (Brillouin frequency shift) of Ω_B and a gain linewidth (Brillouin linewidth) of Γ_B. Subsequently, the pump light is reflected by a 0° mirror behind the medium cell, and the leading edge of the waveform will meet and interact with its subsequent part in the Brillouin medium cell in a completely collinear state. If the normalized intensity ratio of the initial Stokes light component exceeds 10^{-12}, the Stokes component in the reflected pump beam can extract the energy of the incident pump light, thus achieving pulse width compression. The frequency distribution $f(v)$ of the pump light and the normalized intensity ratio η of the initial Stokes component are shown in Figure 2. The value of η is calculated by Equation (1):

$$\eta = \frac{\int_{\Omega_B-\Gamma_B/2}^{\Omega_B+\Gamma_B/2} f(v)\mathrm{d}v}{\int_0^{\infty} f(v)\mathrm{d}v}. \quad (1)$$

Firstly, the relationship between η and the pump pulse width is simulated, as shown in Figure 3. As the pump pulse width increases, η continuously decreases. When the pump pulse width increases to 5.5 ns, η decreases to 6.285×10^{-22} and then remains unchanged. Figure 4 illustrates the time-domain waveforms and corresponding changes in η for different pump pulse widths. The results show that when the pump pulse width is 5.5 ns, the effective frequency range of its spectrum no longer contains the Stokes component, and the η at this time is entirely provided by the thermal noise generated by the zero-point effect of the medium molecules. Therefore, it no longer changes with variations in pump pulse width. Meanwhile, when the pump pulse width is 0.5 ns, η reaches 7.78×10^{-12}, which indicates that transient SPBS can theoretically achieve effective pulse compression.

Furthermore, the variation of η with pump intensity in different Brillouin media is simulated, with a diameter of pump spot of 3 mm, as shown in Figure 5(a). Simulation results show that in the initial stage of increased pump intensity, the phonon field starts to build up and strengthen from thermal noise, and η shows a rapid increasing trend. As the pump intensity continues to increase, when the sound field amplitude reaches saturation, the pump intensity is much greater than the sound field intensity, at which point η gradually tends to stabilize. This is because as the pump

https://doi.org/10.1017/hpl.2026.10160 Published online by Cambridge University Press

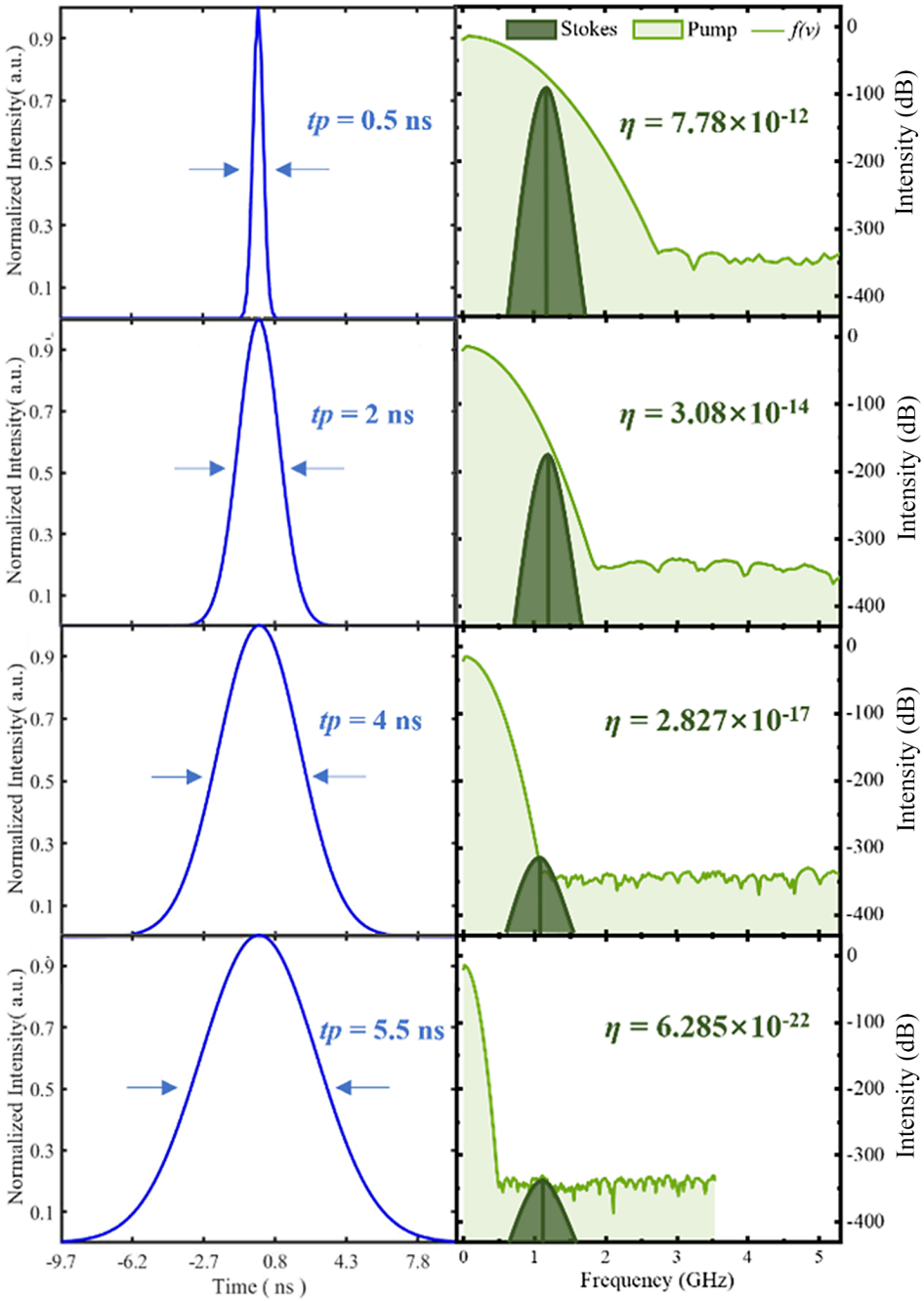


Figure 4. Time-domain waveforms of different pump pulse widths and the variation of η in the corresponding spectrum.

energy increases, the intensities of all modal components within the pump light spectrum rise; the specific distribution of this energy is described by a convolution process within the coupled-wave equations. In other words, the normalized intensity ratio referred to conceptually is also modulated by the pump intensity in practice. Considering the influence of heat accumulation at high repetition rates on the scattering process, the variation of η with temperature was investigated, as shown in Figure 5(b). As the temperature increases, η continuously decreases. This is because as the temperature increases, the kinematic viscosity decreases, and the Brillouin linewidth of the medium decreases accordingly. The optical properties of the Brillouin medium used are shown in Table 1.

Based on previous simulation results, a pump pulse width of 0.5 ns and a maximum pump energy of 30 mJ are selected. The output pulse width of the transient SPBS is simulated as a function of pump intensity, as shown in Figure 6. The results show that pulse width compression occurred in all four selected Brillouin media, with the

https://doi.org/10.1017/hpl.2026.10160 Published online by Cambridge University Press

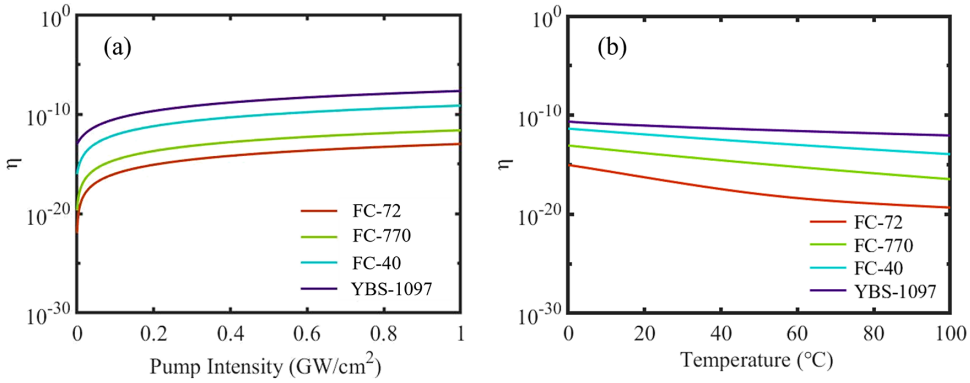


Figure 5. Variation of η with pump intensity and temperature in different media: (a) pump intensity; (b) temperature.

Table 1. Partial optical properties of the selected Brillouin media.

Medium	Absorption coefficient α (cm^{-1}) (300 Hz)	Brillouin linewidth Γ_B (MHz)	Brillouin frequency shift ω_B (MHz)
FC–72	3.92×10^{-3}	270	1100
FC–770	3.65×10^{-3}	575	1081
FC–40	3×10^{-3}	1292	1386
YBS–1097	1.5×10^{-3}	7235	1585

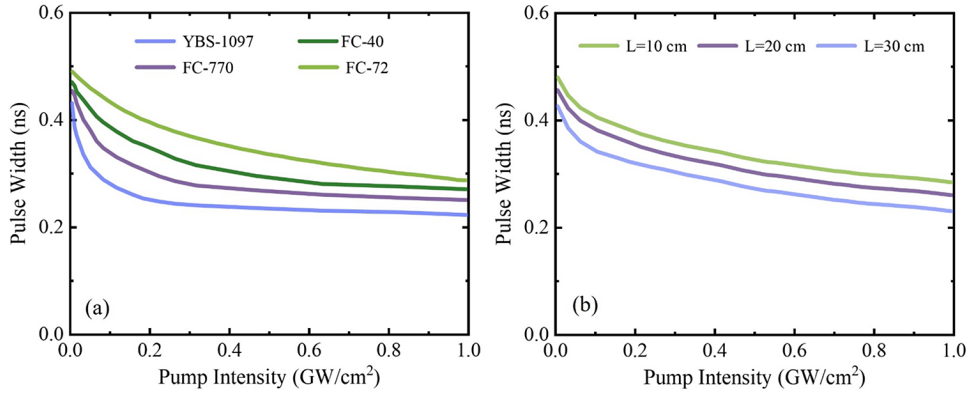


Figure 6. Variation of output pulse width with pump intensity: (a) different media; (b) different interaction lengths.

narrowest compressed pulse width, approximately 230 ps, obtained in YBS-1097, as shown in Figure 6(a). This is because of its larger Brillouin linewidth and faster sound field setup. Meanwhile, the greater the interaction length, the smaller the compression pulse width, which is consistent with the traditional SBS pattern, as shown in Figure 6(b). In summary, the simulation results demonstrate that the pump pulse width is the key factor determining η, and the transient SPBS with a pump pulse width of 0.5 ns has significant compression capacity. On the other hand, η is the core parameter that determines the compression characteristics of transient SPBS. The variation of η with temperature proves that the heat accumulation problem caused by the high repetition rate will restrict the output characteristics of transient SPBS.

3. Experimental setup

A schematic diagram of the optical path of the high-repetition-rate transient SPBS pulse compression system is shown in Figure 7. The seed source is self-built passively *Q*-switched microchip single longitudinal mode (SLM) laser with an adjustable repetition rate of 1–1000 Hz, pulse width of 480 ps and single pulse energy of 60 μJ. The time-domain waveform and corresponding spectrum are shown in Figure 8. The isolator (ISO) is placed between the seed source and the amplifier to prevent backscattered light during the SPBS process from damaging the seed source. After the pump light passes through amplifiers AMP1 and AMP2, the energy is amplified to 7 mJ. Two quarter-wave plates, QP1 and QP2, form a 'twisted pendulum' to improve the spatial

https://doi.org/10.1017/hpl.2026.10160 Published online by Cambridge University Press

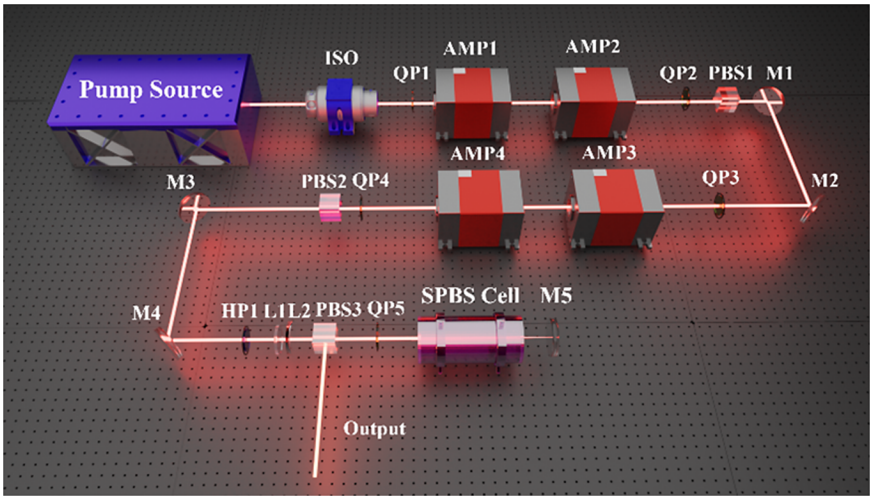


Figure 7. Schematic diagram of the experimental optical path.

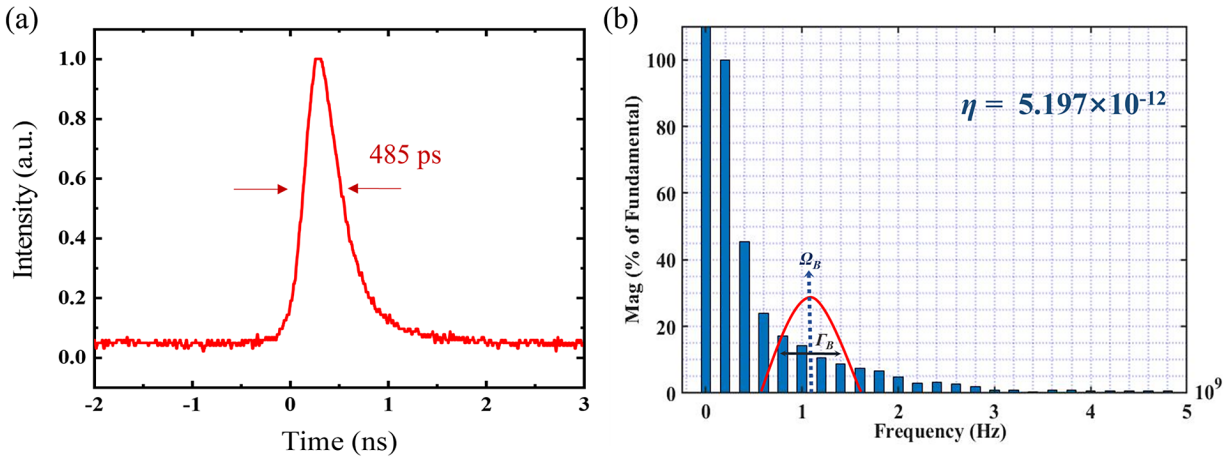


Figure 8. Time-frequency characteristics of pump light: (a) time-domain waveform; (b) η of the spectrum.

distribution uniformity of energy extraction and compensate the deterioration effect of thermal depolarization on spot morphology. PBS1 is used to filter out the depolarization component to ensure the polarization degree of laser. The laser is amplified to 60 mJ by AMP3 and AMP4, then passes through the energy regulator composed of half-wave plate HP1 and PBS3 after thermal depolarization compensation and depolarization filtering, and enters the SPBS compression system through the quarter-wave plate QP5. We place high-reflection mirror M5 behind the medium cell, which is close to the rear window mirror of the medium cell to avoid the waste of effective length. During the experiment, the effective energy of the reflected pump light was varied by adjusting the reflectivity of mirror M5 to investigate its influence on the compression capability of SPBS. The collinear reflection of the incident pump light allows its leading edge to interact with the subsequent portion, and the compressed short-pulse light is output through PBS3.

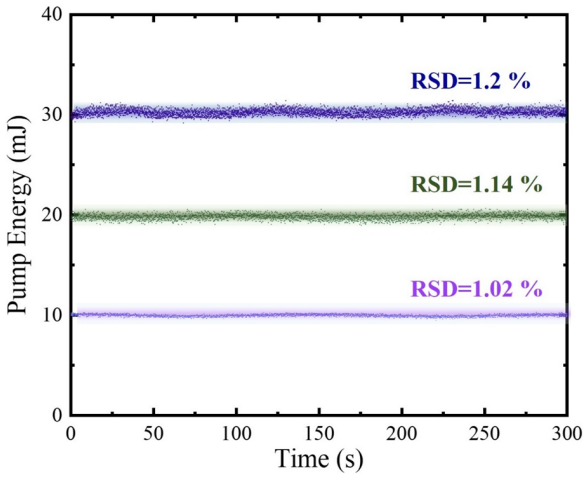


Figure 9. RSD of different pump energies.

Since energy stability is one of the research focuses of this study, in order to eliminate the influence of energy fluctuations of the pump light on the experimental results, we

https://doi.org/10.1017/hpl.2026.10160 Published online by Cambridge University Press

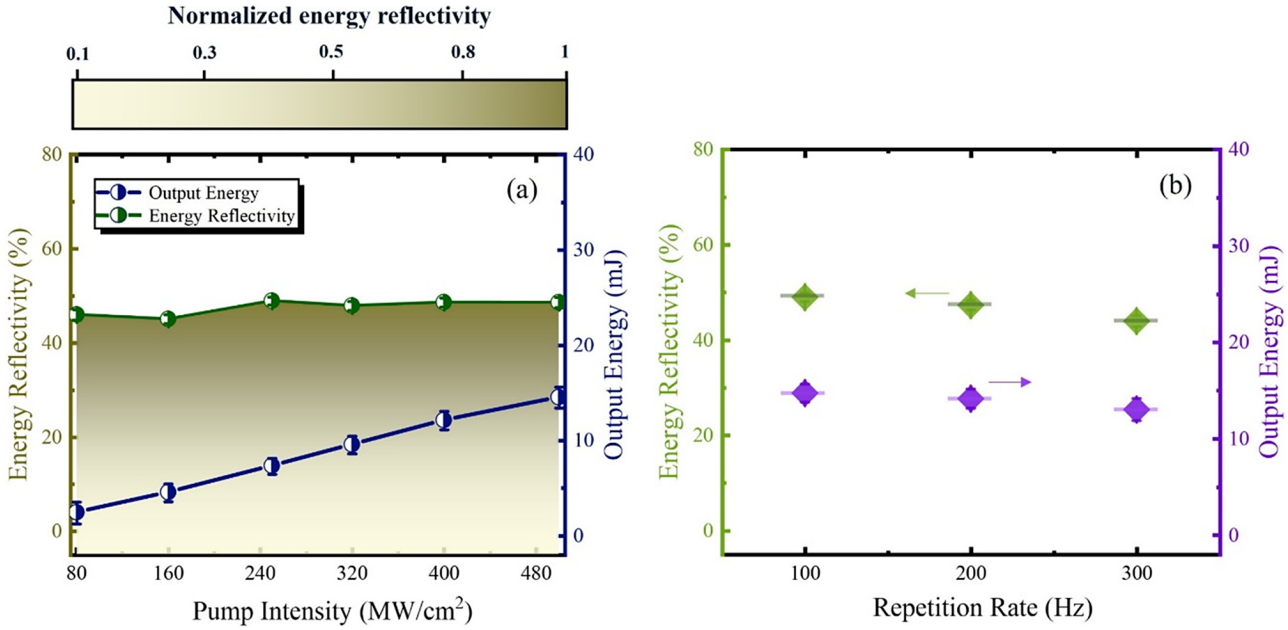


Figure 10. Variation of energy reflectivity and output energy with pump parameters: (a) pump intensity; (b) repetition rate.

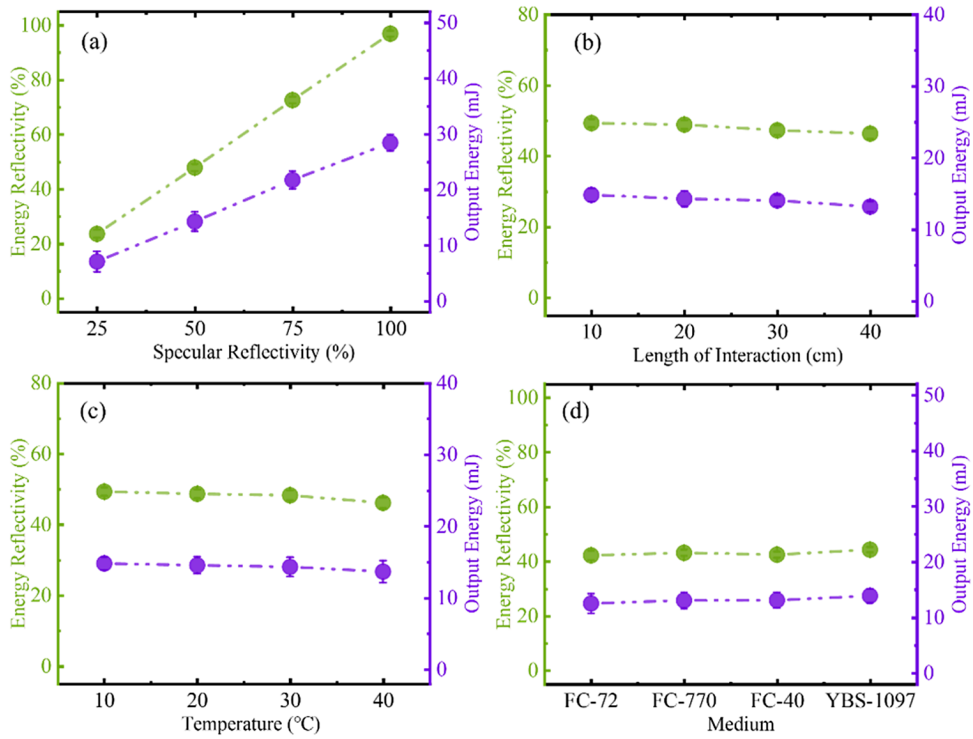


Figure 11. Variation of energy reflectivity and output energy with structural and medium parameters: (a) specular reflectivity; (b) interaction length; (c) temperature; (d) medium.

measure the RSD of different pump energies at a repetition rate of 300 Hz, as shown in Figure 9. An increase in pump energy results in a slight rise in RSD, which may be due to the amplified spontaneous emission (ASE) effect caused by the increased pump power of the laser diode (LD) amplifier or a minor impact of temperature changes on its stability. The pump energy was continuously measured for more than 5 minutes (about 10,000 pulses) using an energy meter (Vega Pyroelectric PE-50-DIF-E, Ophir Optronics, Israel) to obtain the standard deviation reading. Then, a set of RSD1 values was calculated. The average value of five sets of measurements was taken as the final energy RSD. All RSDs presented in this paper follow this measurement method.

https://doi.org/10.1017/hpl.2026.10160 Published online by Cambridge University Press

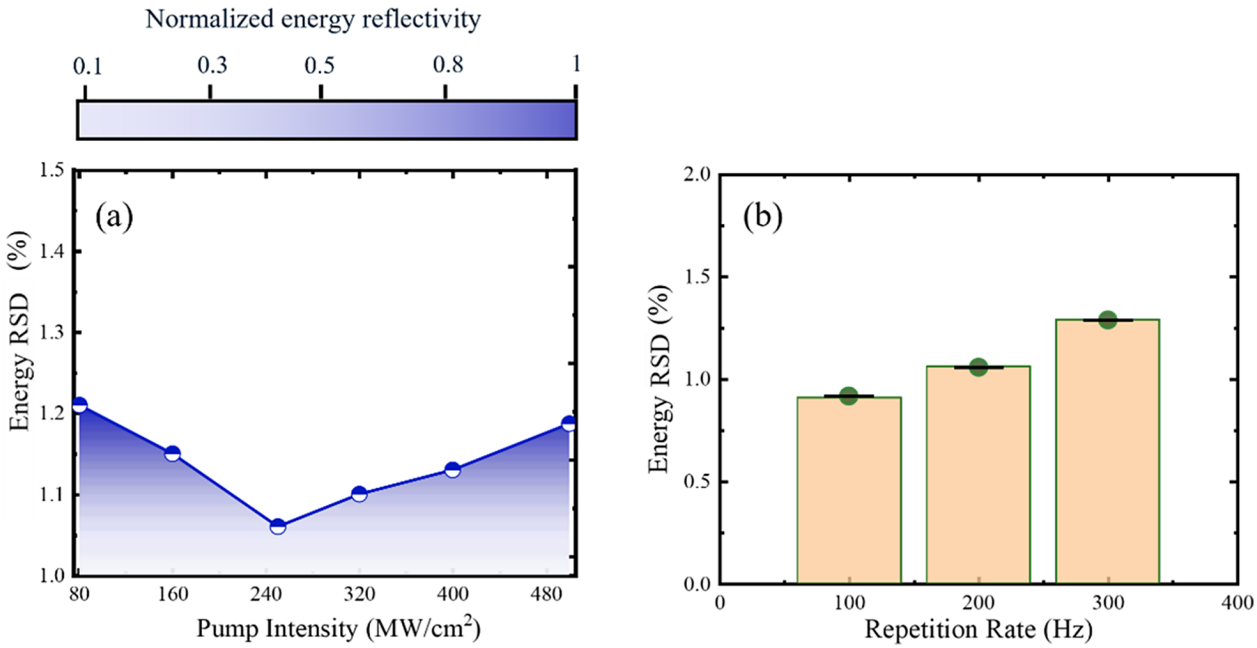


Figure 12. Variation of energy RSD with pump parameters: (a) pump intensity; (b) repetition rate.

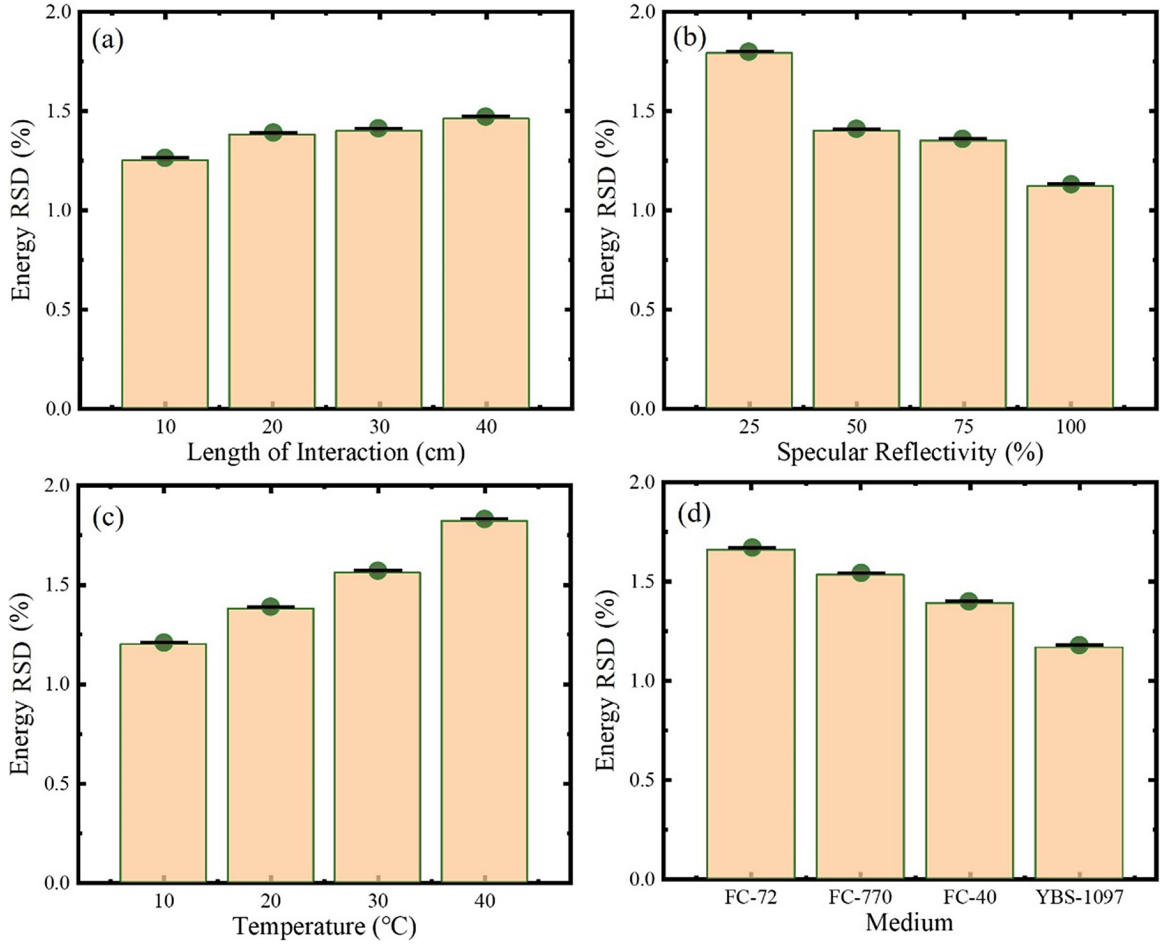


Figure 13. Variation of energy RSD with structural and medium parameters: (a) interaction length; (b) specular reflectivity; (c) temperature; (d) medium.

https://doi.org/10.1017/hpl.2026.10160 Published online by Cambridge University Press

4. Results

Firstly, when the reflectivity of M5 is 50%, the changes in energy reflectivity and output energy with pump intensity are measured at a repetition rate of 100 Hz, as shown in Figure 10(a). The results show that as the pump intensity increases, the energy reflectivity remains basically unchanged at about 48%. The output energy shows a linear growth trend, and the energy loss is due to the absorption of the medium and the reflection of the window mirror. As the repetition rate increases to 300 Hz, the energy reflectivity gradually decreases to 46%, which is due to the increase in medium absorption, as shown in Figure 10(b). Figure 11 illustrates the variation of energy reflectivity and output energy with different structural and medium parameters at a repetition rate of 300 Hz.

The results show that the output energy and reflectivity are determined by the mirror reflectivity, as shown in Figure 11(a). Due to the influence of medium absorption, they decrease slightly with the increase of the interaction length and temperature, as shown in Figures 11(b) and 11(c). In YBS-1097, the medium with the lowest absorption coefficient, the energy reflectivity can reach approximately 48.5%, which is 4% higher than that in FC-72, as shown in Figure 11(d). The temperature of the medium is regulated by an external water-cooling system.

The variation of energy stability RSD with pump intensity and repetition rate is investigated, as shown in Figure 12. As the pump intensity increases, the RSD shows a trend of first decreasing and then increasing, with the pump intensity corresponding to the inflection point being approximately 240 MW/cm^2. Within the low-intensity range, increasing the pump intensity can raise η, thereby improving the stability of the SPBS process. When the pump intensity is too high, the intensity of the SBS-Stokes seed light, which originates from thermal noise, increases and competes with the Stokes component in the pump light, causing the acoustic field stability to deteriorate and the RSD to increase, as shown in Figure 12(a). Meanwhile, as the repetition rate increases, the interference of thermal noise becomes more severe, and the RSD continues to rise, as shown in Figure 12(b). Figure 13 shows the variation of energy RSD under different structural and medium parameters. As the temperature increases, the RSD rises from 1.17% to 1.85%, which indicates the deteriorating effect of thermal accumulation on the scattering process, as shown in Figure 13(c). As the specular reflectivity and Brillouin linewidth increase, η rises accordingly. Before the effective intensity of the SBS-Stokes seed light is excited, the RSD shows a decreasing trend, as shown in Figures 13(b) and 13(d).

Ultimately, we select a high-reflectivity mirror with a reflectivity of 99.9% as the feedback source for the high-repetition-rate transient SPBS compression process. The effective interaction length of 10 cm and the temperature of YBS-1097 of 10°C are used. The laser output achieved an average energy reflectivity of approximately 95% and an RSD of 1.42%, as shown in Figure 14. The results show that in transient SPBS with low pump intensity, even with the enhancement effect of thermal accumulation, the optical breakdown is completely avoided and the energy stability is not significantly degraded. Meanwhile, due to the high feedback effect of the reflector, the transmission loss of SPBS is almost zero, and the system loss comes only from the medium absorption effect. The problem of low energy reflectivity caused by transient effects is also solved. However, as a pulse width compression technology,

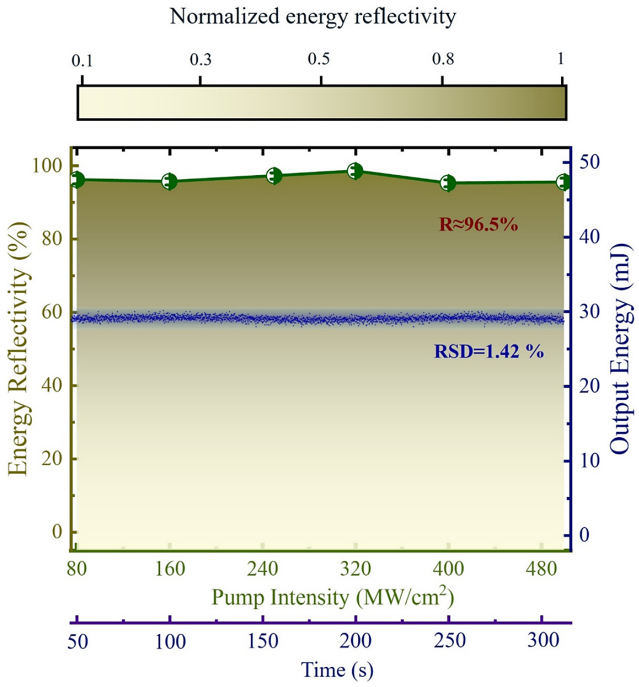


Figure 14. Output energy reflectivity and RSD of high-repetition-rate transient SPBS.

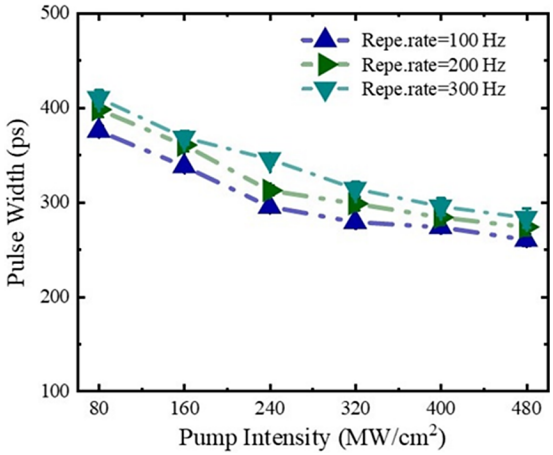


Figure 15. Variation of compression pulse width with pump intensity at different repetition rates.

https://doi.org/10.1017/hpl.2026.10160 Published online by Cambridge University Press

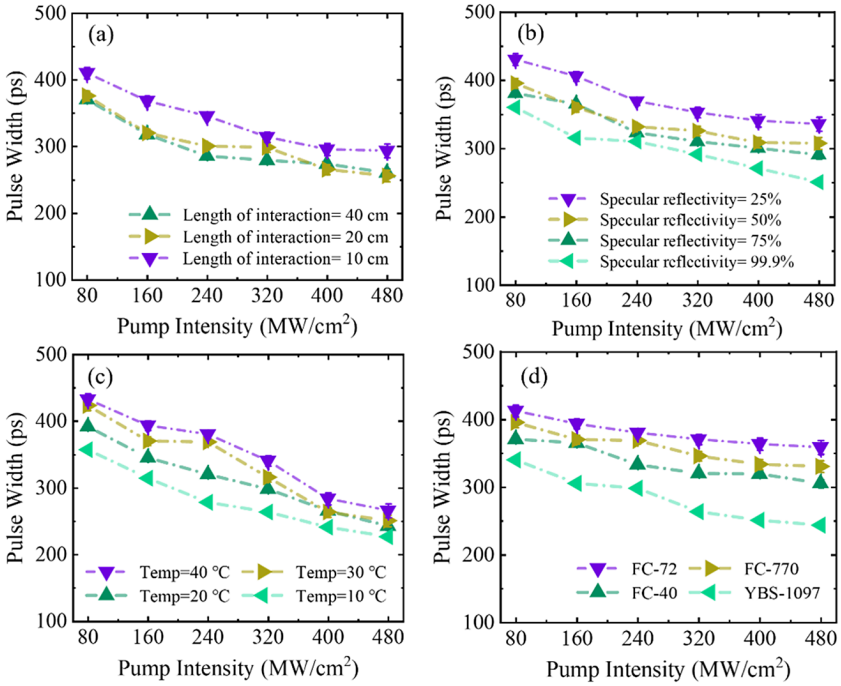


Figure 16. Variation of compression pulse width with structural and medium parameters: (a) interaction length; (b) specular reflectivity; (c) temperature; (d) medium.

its compression capability is the core parameter that needs to be focused on.

To verify the compression capacity of the high-repetition-rate transient SPBS, the evolution of the output pulse width with pump intensity at different repetition rates is investigated experimentally, as shown in Figure 15. As the pump intensity increases, the output pulse width shows a continuous decreasing trend, and it has not yet reached saturation within the existing pump intensity range. If the pump intensity is further increased, the compression pulse width can be further reduced, but the stability may deteriorate. As the repetition rate increases, the compression pulse width widens slightly, which is due to the decrease in kinematic viscosity of the medium in the interaction zone caused by heat accumulation. The compression pulse width is approximately 278 ps $\pm$ 3.5 ps with the pump intensity of 480 MW/cm^2 and the repetition rate of 300 Hz.

Figure 16 illustrates the variation of compression pulse width with different structural and medium parameters. As the interaction length and specular reflectivity increase, the compression pulse width decreases. When the interaction length exceeds 20 cm, the decrease in compression pulse width becomes insignificant. With an interaction length of 20 cm and a specular reflectivity of 99.9%, the minimum compression pulse width is approximately 248.6 ps, as shown in Figures 16(a) and 16(b). As the temperature decreases, the compression pulse width decreases accordingly, as shown in Figure 16(c). In YBS-1097, the compression pulse width decreases significantly, as shown in Figure 16(d). The results in Figures 15 and 16 show that transient SPBS can achieve effective pulse width compression, with a compression ratio of approximately 2, and has not reached saturation.

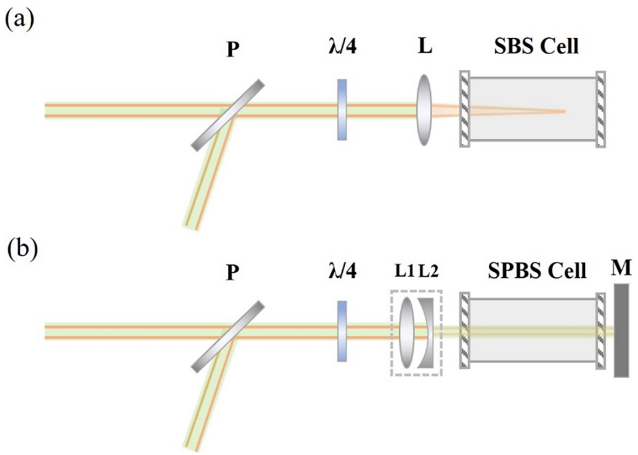


Figure 17. Schematic diagram of the compressed structure of SBS and SPBS: (a) SBS; (b) SPBS.

In order to emphasize the improving effect of transient SPBS on the degradation of energy characteristics caused by transient effects and thermally induced breakdown enhancement effects, we conduct a comparative study on the output characteristics of SBS and SPBS under the same experimental conditions; a schematic diagram of the compression system is shown in Figure 17. The SBS employs a focusing structure with a focal length of 200 mm for lens L and a size of focal spot of approximately 400 μm, as shown in

https://doi.org/10.1017/hpl.2026.10160 Published online by Cambridge University Press

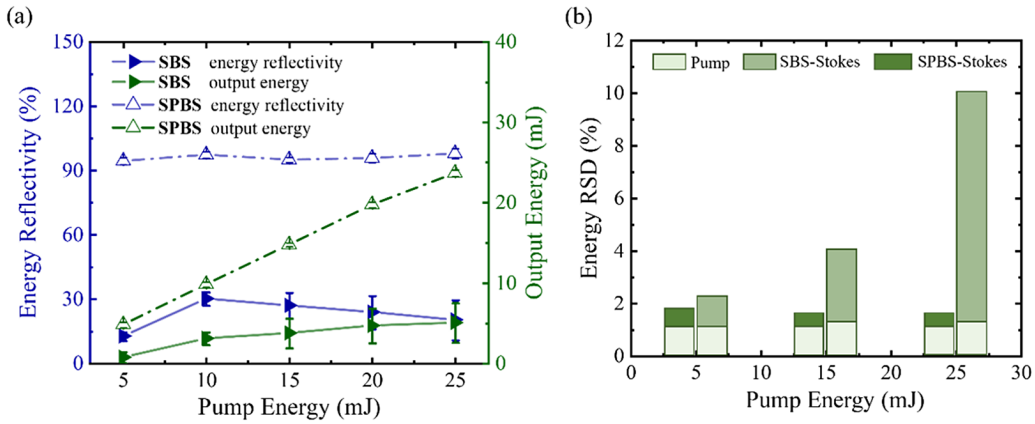


Figure 18. Comparison of output energy (reflectivity) and stability between SBS and SPBS: (a) output energy (reflectivity); (b) stability.

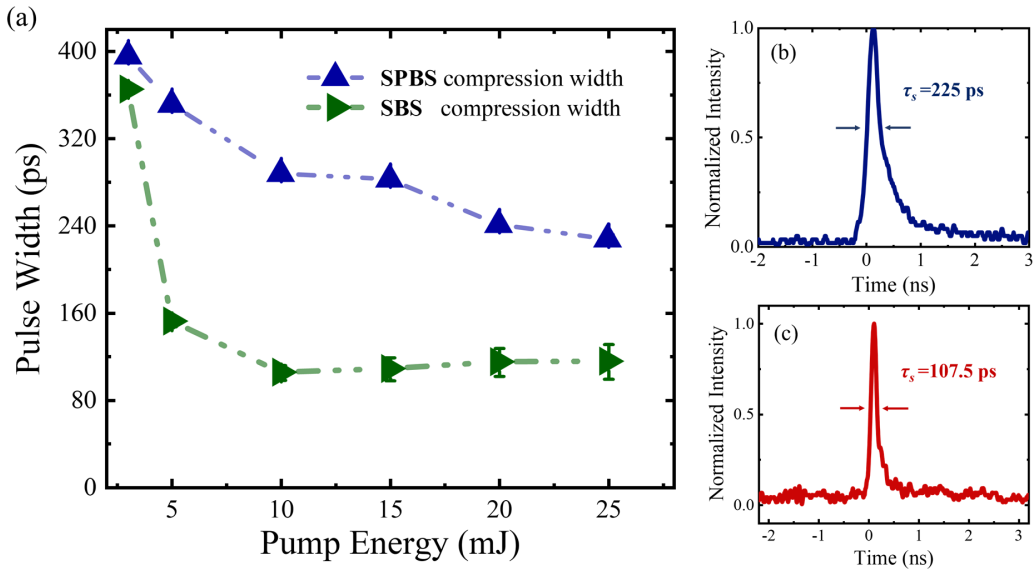


Figure 19. Comparison of compressed pulse width and time-domain waveforms of SBS and SPBS: (a) compressed pulse width; (b) output time-domain waveform of SPBS; (c) output time-domain waveform of SBS.

Figure 17(a). The SPBS system employs a beam-shrinking structure with a magnification of 1.5, and adds a 0° high-reflectivity mirror M behind the medium cell to reflect the incident pump light, as shown in Figure 17(b). The waist of the pump beam is 3 mm, the length of the medium cell is 200 mm and the reflectivity of M is 99.5%. The repetition rate is 300 Hz, the pump energy is 5–25 mJ and the Brillouin medium selected is YBS-1097.

Figure 18 illustrates a comparison of the output energy (reflectivity) and stability of SBS and SPBS. Due to the special structural design of SPBS, it completely overcomes the effects of optical breakdown and transient effects, with energy reflectivity basically stable at 95% and a maximum output energy of 24.1 mJ. For SBS, due to the high system loss caused by transient effects and severe optical breakdown, the energy reflectivity is limited to below 35%, and the maximum output energy is only 6 mJ, as shown in Figure 18(a). Figure 18(b) shows a comparison of the energy stability of systems, including the energy RSD of the pump light itself. When the pump energy is 5 mJ, the degree of instability additionally introduced by the SBS and SPBS compression processes is basically the same. When the pump energy increases to 15 mJ, a slight breakdown effect appears in the SBS process, and the RSD increases. The pump intensity of SPBS is far from reaching the breakdown threshold, and due to the increase in pump energy, η increases, making the scattering process more stable. When the pump energy is 25 mJ, the breakdown effect in SBS is already very severe, and the energy RSD surges to 8.2%, while that in SPBS is only 1.42%. The results show that high-repetition-rate transient SPBS can achieve high output energy with minimal energy loss and introduces little additional instability relative to the pump light.

The saturation compression pulse width of SBS is about half that of SPBS, as shown in Figure 19. This is a direct result of the difference in their scattering intensities. The

https://doi.org/10.1017/hpl.2026.10160 Published online by Cambridge University Press

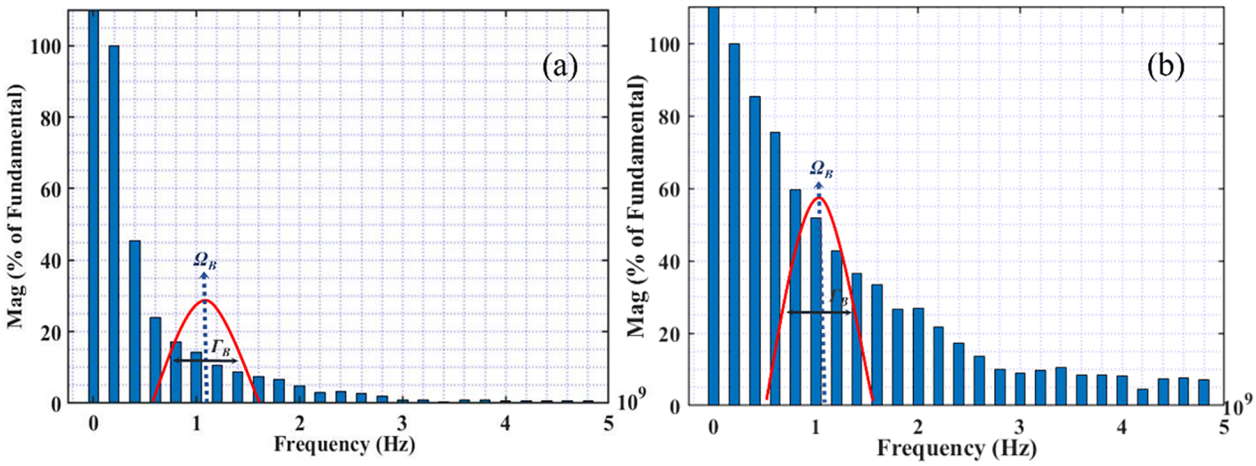


Figure 20. Spectra of pump light and reflected light: (a) pump light; (b) reflected light.

scattering intensity in the Rayleigh region of the SBS process is significantly higher than that of the SPBS process, resulting in a greater number of scattered photons per unit time, more significant contrast between the leading and trailing edges of the waveform and a narrower compressed pulse width. During the SPBS process, when the pump energy is increased to 25 mJ, the compression pulse width is approximately 225 ps, but compression saturation is not reached, as shown in Figure 19(b). Figure 20 illustrates the spectral distribution of the incident pump light and the reflected light; it can be observed that, within the Brillouin linewidth, the relative intensity of the modal components in the reflected light spectrum is significantly enhanced compared to that of the pump light. This phenomenon demonstrates that the Stokes component of reflected light has significant amplification. Theoretically, if the pump energy continues to increase, the normalized proportion of the initial Stokes component will gradually be occupied by the Stokes seed light originating from thermal noise and the output light from SPBS will coexist with the SBS-Stokes light. However, in actual structures, there is a fixed time delay between the two beams, which may cause waveform distortion. The results show that, due to limitations in scattering intensity, the compression capacity of SPBS is significantly lower than that of SBS.

5. Conclusion

In summary, this study proposes a high-repetition-rate transient SPBS pulse compression technique, aiming to solve the problem of decreased energy reflectivity and stability caused by the combined transient effect and optical breakdown effect in the traditional SBS process. Through simulation and experimental studies, the physical mechanism of using self-feedback seed light to compensate for scattering gain is revealed. The important conclusion that transient SPBS can achieve effective compression under low laser flux is verified. The results show that when a high-reflectivity mirror is used as the feedback source, the system loss comes only from the absorption of the medium and the reflection of the window film. The thermal absorption enhancement effect introduced by the repetition rate increase will cause the loss to increase and the stability to decrease. Due to the extremely low pump intensity, no breakdown effect occurs in the SPBS process even with heat accumulation. Ultimately, a maximum output energy of 24.1 mJ@300 Hz is achieved with an average energy reflectivity of 95%, nearly doubling the peak laser power with extremely low energy loss, and realizing stable output of a high-repetition-rate short-pulse laser with an energy RSD of only 1.42%.

Acknowledgements

This work was supported by the National Key R&D Program of China (Grant No. 2024YFB3613600) and the Natural Science Foundation of Hebei Province (Grant Nos. F2023202082 and F2022202035).

References

1. M. Spellauge, C. Doñate-Buendía, S. Barcikowski, B. Gokce, and H. P. Huber, Light: Sci. Appl. **11**, 68 (2022).
2. G. Conner and A. Bedros, in *Optica Nonlinear Optics Topical Meeting* (Optica Publishing Group, 2023), paper M4A.6.
3. J. F. McGarry, E. D. Hoffman, J. J. Degnan, J. W. Cheek, C. B. Clarke, I. F. Diegel, H. L. Donovan, J. E. Horvath, M. Marzouk, A. R. Nelson, D. S. Patterson, R. L. Ricklefs, M. D. Shappirio, S. L. Wetzel, and T. W. Zagwodzki, J. Geod. **93**, 2249 (2018).
4. J. Y. Zhang, R. Wang, X. Zhu, A. F. Pan, C. X. Han, X. Li, D. Zhao, C. S. Ma, W. J. Wang, H. B. Su, and C. M. Niu, Nat. Commun. **8**, 683 (2017).
5. Y. Qi, S. Yao, Z. X. Du, J. R. Zhang, C. Y. Zhou, X. H. Fu, H. Li, T. Mi, Y. H. Chen, Y. F. Wang, Y. Luo, X. Y. He, J. Nan, Y. J. Zhang, L. Sun, P. Xia, S. Q. Cai, J. L. Du, J. J. Xie, W. B. Chen, and F. Yang, Nat. Photonics **19**, 879 (2025).
6. A. M. Rodin, A. Cerneckyte, P. Mackonis, and A. Petrulenas, Photonics **10**, 1060 (2023).

https://doi.org/10.1017/hpl.2026.10160 Published online by Cambridge University Press

7. C. Cao, Y. L. Wang, Q. F. Dang, J. F. Yue, L. R. He, H. Z. Yu, Y. Yu, and Z. W. Lu, Chin. Opt. Lett. **24**, 071409 (2026).
8. A. I. Erokhin, V. I. Kovalev, and F. S. Faizullov, Sov. J. Quantum Electron. **16**, 872 (1986).
9. D. Pohl and W. Kaiser, Phys. Rev. B **1**, 31 (1970).
10. H. Yoshida, H. Fujita, M. Nakatsuka, T. Ueda, and A. Fujinoki, Laser Part. Beams **25**, 481 (2007).
11. H. Yoshida, T. Hatae, H. Fujita, M. Nakatsuka, and S. Kitamura, Opt. Express **17**, 13654 (2009).
12. V. Kmetik, H. Fiedorowicz, A. A. Andreev, K. J. Witte, H. Daido, H. Fujita, M. Nakatsuka, and T. Yamanaka, Appl. Opt. **37**, 7085 (1998).
13. V. Kmetik, V. H. Yoshida, H. Fujita, M. Nakatsuka, and T. Yamanaka, Proc. SPIE **3889**, 818 (2000).
14. Z. H. Liu, R. Fan, D. Jin, T. T. Luo, S. S. Li, N. Li, S. W. Li, Y. L. Wang, and Z. W. Lu, Opt. Express **30**, 12586 (2022).
15. Z. H. Liu, Y. L. Wang, Z. X. Bai, Y. R. Wang, D. Jin, H. L. Wang, H. Yuan, D. Y. Lin, and Z. W. Lu, Opt. Express **26**, 23051 (2018).
16. J. K. Kang, H. B. Zhang, X. C. Yan, Y. Lang, and Z. W. Fan, Chin. Opt. **11**, 736 (2018).
17. H. L. Wang, S. W. Cha, H. J. Kong, Y. L. Wang, and Z. W. Lu, Opt. Express **30**, 38995 (2022).
18. J. F. Yue, Y. L. Wang, M. Y. Jia, K. Li, C. Cao, Y. Yu, Y. F. Li, and Z. W. Lu, High Power Laser Sci. Eng. **11**, e70 (2023).
19. C. Cao, Y. L. Wang, J. F. Yue, Z. B. Meng, K. Li, Y. Yu, Z. X. Bai, and Z. W. Lu, Opt. Express **30**, 33721 (2022).
20. J. K. Kang, Z. W. Fan, Y. T. Huang, H. B. Zhang, W. Q. Ge, M. S. Li, X. C. Yan, and G. X. Zhang, Opt. Express **26**, 6560 (2018).
21. H. L. Wang, S. W. Cha, H. J. Kong, Y. L. Wang, and Z. W. Lu, Opt. Express **27**, 9895 (2019).
22. Y. F. Chen, B. W. Tan, D. Jin, B. Chen, Z. X. Bai, K. Wang, Y. L. Wang, and Z. W. Lu, High Power Laser Sci. Eng. **12**, e20 (2024).
23. H. L. Wang, S. W. Cha, H. J. Kong, Y. L. Wang, and Z. W. Lv, High Power Laser Sci. Eng. **10**, e24 (2022).
24. H. L. Wang, S. W. Cha, H. J. Kong, Y. L. Wang, and Z. W. Lu, Opt. Express **27**, 29789 (2019).
25. S. F. Guo, Q. S. Lu, X. A. Cheng, P. Zhou, and Y. Yin, Acta Phys. Sin. **53**, 1831 (2004).
26. A. S. Dement'ev, I. Diomin, E. Murauskas, and N. Slavinskis, Quantum Electronics. **41**, 153 (2011).
27. X. H. Zhu, Z. W. Lu, Y. L. Wang, H. K. Zhang, in *CLEO: Applications and Technology* (Optica Publishing Group, 2015), paper JTh2A.97.
28. Y. L. Wang, X. H. Zhu, Z. W. Lu, and H. K. Zhang, Opt. Express **23**, 23318 (2015).
29. R. W. Boyd and K. Rzazewski, Phys. Rev. A **42**, 5514 (1990).

https://doi.org/10.1017/hpl.2026.10160 Published online by Cambridge University Press